行政院國家科學委員會專題研究計畫 期末報告

密度泛函數理論(DFT)對於一些化學系統的精確性

計 畫 類 別 ：個別型
計 畫 編 號 ：NSC 101-2113-M-040-004-
執 行 期 間 ：101 年 08 月 01 日至 102 年 10 月 31 日
執 行 單 位 ：中山醫學大學應用化學系（所）

計 畫 主 持 人 ：賴金宏

公 開 資 訊 ：本計畫涉及專利或其他智慧財產權，1 年後可公開查詢

中 華 民 國 102 年 12 月 23 日

中 文 摘 要 ： 由於其價格層的 ns 以及 np 軌域是全填滿的,所以位於元素週期表中的第 18 族元素通稱為稀有氣體,它們具有極低的化學反應性。它們通常以單原子物種存在。它們分別為氦(He)、氖(Ne)、 氬(Ar)、氪(Kr)、氙(Xe),以及氡(Rn),而相較於氦、氖、氬、氪(Kr),和氙而言,氡這個元素具有輻射活性。惰性氣體的游離能相較於其他族元素是最高的,並且它們也沒有接受額外電子的傾向。因此,它們也被稱為惰性氣體。然而在 1962 年,英國化學家尼爾巴特利特(Neil Bartlett)推翻了長久以來對這類氣體的惰性性質的觀點,他發現當氙氣暴露於六氟化鉑(PtF6)時會產生一種含有氙的化合物(Xe+[PtF6]-)。此後,一些含有氙或其他稀有氣體的化合物就被陸續的發現。例如,XeF4、XeO3、XeO4、XeOF4 和 KrF2。除了氡具有輻射活性之外,氙可說是這族元素中化學活性最高的一個元素。可能由於具有比較高的化學活性,氙在自然界的含量遠較預期值小了 20 倍。此預期值是由其他存在於自然界中的稀有氣體之含量所推估得。二氧化氙(XeO2)的發現正好可以解釋為什麼氙如何’神秘’地消失了?雖然也有人對於氙的枯竭提出了四種可能,這四種可能包括了冰的包封(entrapment in ices),水包合物(water clathrates),沉積物(sediments),以及由早期大氣逸散 (early escape from the atmosphere),但這四個假設隨即被證明是站不住腳的。由 2005 年 Sanloup 等人所做的一系列高壓 X-射線干涉(x-ray diffraction)的實驗結果可知氙可能吸附於位於地表下好幾公里的石英上。在今年,2011 年,二氧化氙這個物質被成功地合成出來並且以光譜方法檢測其性質 [7]。拉曼光譜和 16/180 同位素富集(16/180 enrichment)實驗都表明,XeO2 擁有一個擴展的結構 (extended structure),其中氙的氧化數是四價並以四個鄰近的氧原子當作橋樑與其他單體鍵結。 根據價殼層電子對的排斥(valence shell electron pair repulsion； VSEPR),它應該屬於 AX4E2 的排列(其 中 X 表電子對而 E 表示孤對電子對)而呈現平面四邊形(square plane)的幾何結構。所以我們擬以密度泛函數理論來探討這類平面四邊形的氙化合物。

中文關鍵詞： 稀有氣體, 二氧化氙, 拉曼光譜, 16/180 同位素富集, 平面四邊形

英 文 摘 要 ： Noble gases, which comprise the 18th group of the periodic table, possess completely filled outer ns and np subshells and exhibit characteristically low chemical reactivity. These gases generally exist as monatomic species. The six naturally occurring noble

gases in group 18 are He, Ne, Ar, Kr, and Xe, whereas Rn is a radioactive element. Among the elements,the noble gases exhibit the highest ionization energies and are resistant toward accepting extra electrons and hence are also referred to as inert gases.
In 1962, the British chemist Neil Bartlett challenged a longheld view of the nonreactivity of these elements when he exposed xenon to platinum hexafluoride and formed the complex assemblage XeF+[PtF6]-4 Since then, a number of compounds containing xenon or other noble gases have been prepared, including XeF4, XeO3, XeO4, XeOF4, and KrF2. Recently, it was discovered that xenon dioxide (XeO2), the so called missing xenon oxide, can be synthesized and definitively characterized using spectroscopy.5,6 This finding accounts for the nondetection of atmospheric xenon, even though it was thought to have been present when the Earth was created.7,8
Theoretically, xenon depletion has been attributed to entrapment in ice, water clathrates, and sediments and early escape from the atmosphere； however, these hypotheses are
untenable.9-2 Sanloup et al. proposed that Xe may be retained within silicate minerals and SiO2 as XeO2.5 Both Raman spectroscopy and 16/180 isotopic enrichment studies have indicated that XeO2 has an extended structure in which Xe(IV) is oxygen-bridged to four neighboring oxygen atoms.6 On the basis of valence shell electron pair repulsion
(VSEPR) theory, XeO2 belongs to the AX4E2 arrangement and adopts a local square-planar XeO4 geometry. In contrast,Xe(VIII) assumes a tetrahedral geometry when bound to four
oxygen atoms. The vast applicability of noble gases warrants more in-depth understanding of the chemical properties of the group 18 elements. Thus, herein, we investigate the differences between the four-oxygen-bound Xe(IV) and Xe(VIII) species.

英文關鍵詞： noble gases, XeO2, Raman Spectroscopy, 16/180 enrichment, square planar

THE JOURNAL OF PHYSICAL CHEMISTRY A

Article

pubs.acs.org/JPCA

Computational Study of $Xe(OH)_4$, $XeO(OH)_3^-$, and $XeO_2(OH)_2^{2-}$

Chin-Hung Lai*

School of Applied Chemistry, Chung Shan Medical University, 402 Taichung, Taiwan, Republic of China

Supporting Information

ABSTRACT: Because of the vast applicability of noble gases, a more detailed understanding of their chemical properties is necessary. Recently, Brock et al. successfully synthesized XeO_2 and demonstrated that it has an extended structure in which Xe(IV) is oxygen-bridged to four neighboring oxygen atoms using Raman and $^{16/18}O$ isotopic enrichment studies. On the basis of valence shell electron pair repulsion, XeO_2 belongs to the AX_4E_2 arrangement and assumes a local square-planar XeO_4 geometry. In contrast, Xe(VIII) assumes a tetrahedral geometry when bound to four oxygen atoms. A theoretical comparison of the four-oxygen-bound Xe(IV) and Xe(VIII) species, based primarily on the density functional theory functional TPSS1KCIS, is presented herein. The properties of $XeO_n(OH)_{4-n}^{n-}$ species, where n is equal to 0, 1, or 2, were evaluated on this basis, and these results are compared with those of the well-known species XeO_4.

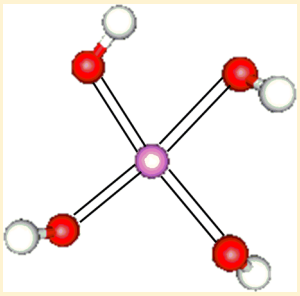

1. INTRODUCTION

Noble gases, which comprise the 18th group of the periodic table, possess completely filled outer *n*s and *n*p subshells and exhibit characteristically low chemical reactivity. These gases generally exist as monatomic species. The six naturally occurring noble gases in group 18 are He, Ne, Ar, Kr, and Xe, whereas Rn is a radioactive element. Among the elements, the noble gases exhibit the highest ionization energies and are resistant toward accepting extra electrons and hence are also referred to as inert gases. Consequently, these gases are used as inert atmospheres in several applications. For example, Ar is used in the synthesis of compounds that are sensitive to nitrogen. Additionally, solid-state argon is used as an inert low-temperature matrix to trap unstable compounds such as reactive intermediates.[1] Because of their lack of chemical reactivity, noble gases are also used in lighting. For example, in halogen lamps, krypton is mixed with small amounts of iodine or bromine compounds.[2] Furthermore, dimers of noble gases, such as Ar_2, Kr_2, or Xe_2, are short-lived electronically excited molecules that are used in excimer lasers, which in turn are used in microlithography, microfabrication, etc. for the manufacture of integrated circuits.[3]

In 1962, the British chemist Neil Bartlett challenged a long-held view of the nonreactivity of these elements when he exposed xenon to platinum hexafluoride and formed the complex assemblage $XeF^+[PtF_6]^-$.[4] Since then, a number of compounds containing xenon or other noble gases have been prepared, including XeF_4, XeO_3, XeO_4, $XeOF_4$, and KrF_2. Recently, it was discovered that xenon dioxide (XeO_2), the so-called missing xenon oxide, can be synthesized and definitively characterized using spectroscopy.[5,6] This finding accounts for the nondetection of atmospheric xenon, even though it was thought to have been present when the Earth was created.[7,8] Theoretically, xenon depletion has been attributed to entrapment in ice, water clathrates, and sediments and early escape from the atmosphere; however, these hypotheses are untenable.[9−12] Sanloup et al. proposed that Xe may be retained within silicate minerals and SiO_2 as XeO_2.[5]

Both Raman spectroscopy and $^{16/18}O$ isotopic enrichment studies have indicated that XeO_2 has an extended structure in which Xe(IV) is oxygen-bridged to four neighboring oxygen atoms.[6] On the basis of valence shell electron pair repulsion (VSEPR) theory, XeO_2 belongs to the AX_4E_2 arrangement and adopts a local square-planar XeO_4 geometry. In contrast, Xe(VIII) assumes a tetrahedral geometry when bound to four oxygen atoms. The vast applicability of noble gases warrants more in-depth understanding of the chemical properties of the group 18 elements. Thus, herein, we investigate the differences between the four-oxygen-bound Xe(IV) and Xe(VIII) species. The properties of the $XeO_n(OH)_{4-n}^{n-}$ species shown in Scheme 1, where n is equal to 0, 1, or 2, were also evaluated, and the obtained results are compared herein with those of the well-known species XeO_4. Cases in which n = 3 and 4 were not considered because they are hypothesized to be unstable due to the potentially strong repulsion between two O^{2-} species. The two isomers for the n = 2 case, which have two OH groups in the *cis* or *trans* positions, are also considered.

2. THEORETICAL METHOD

All calculations were performed using the Gaussian 03 program.[13] The second-order many-body perturbation method (MP2) and several density functional theory (DFT) functionals (BLYP, MPWLYP1W, PBE1W, PBELYP1W, MOHLYP, MOHLYP2, TPSS, TPSSLYP1W, B3LYP, B3P86, B3PW91, MPW1LYP, MPW1PW91, MPW1K, TPSSh, BB1K, MPWB1K, MPW1B95, and TPSS1KCIS) were chosen and combined with the triple-ξ basis set (aug)-cc-pVTZ for hydrogen and oxygen.[14−28] For the element xenon, the small-core pseudopotential of the energy-consistent variety must be considered for

Received: January 20, 2012
Revised: September 18, 2012
Published: September 18, 2012

 © 2012 American Chemical Society

Scheme 1. Schematic Representations of $XeO_n(OH)_{4-n}^{n-}$ (n = 0, 1, and 2)

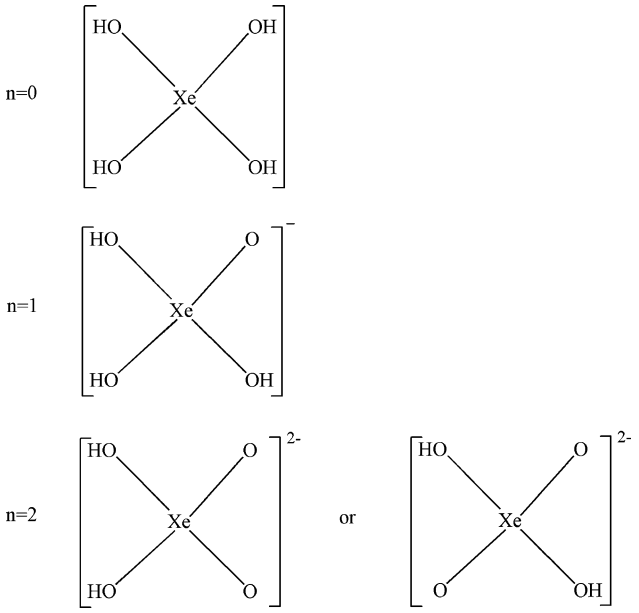

the relativistic effect and is designated as (aug)-cc-pVTZ-PP.[29] The core electron excitations were not included in the current MP2 calculation for conservation of computational resources. Such a simplification has also been used in prior related studies[30] and is acceptable because the core electrons are more inert than the valence electrons. The selected DFT functionals can be categorized into four types as follows: generalized gradient approximations (GGAs; BLYP, MPWLYP1W, PBE1W, PBELYP1W, MOHLYP, and MOHLYP2), meta-GGA (TPSS and TPSSLYP1W), hybrid GGA (B3LYP, B3P86, B3PW91, MPW1LYP, MPW1PW91, and MPW1K), and hybrid meta-GGA (TPSSh, BB1K, MPWB1K, MPW1B95, and TPSS1KCIS). A GGA functional is dependent on the up and down spin densities and their reduced gradients. The combination of the Hartree−Fock exchange and GGA forms a hybrid GGA functional. If a GGA-type DFT functional is also dependent on up and down spin kinetic energy densities, it is called a meta-GGA functional. Similarly, the addition of the Hartree−Fock exchange to a meta-GGA functional forms a hybrid meta-GGA functional. All of the stationary points were positively identified as equilibrium structures; the number of imaginary frequencies (NIMAG) was set to 0. All energetics values were corrected for zero-point vibrational energies. Furthermore, the NBO 5.G function, implemented in Gaussian 03, was used to perform natural bond orbital (NBO) analysis.[31] NBOs are an orthonormal set of localized "maximum occupancy" orbitals; they describe the molecular bonding pattern of electron pairs to yield the most accurate Lewis-like description of the total N-electron density.

3. RESULTS AND DISCUSSION

3.1. Four-Oxygen-Bound Xe(IV) Species $XeO_n(OH)_{4-n}^{n-}$ (n = 0, 1, and 2). On the basis of the optimization of the chosen DFT functionals in this study (see the Supporting Information), the hybrid meta-GGA functional TPSS1KCIS was chosen for execution of the subsequent evaluations. However, to describe the anionic species more accurately, the diffuse functions were added into the chosen basis set in this study (which is designated as aug-cc-pVTZ(-PP)). The TPSS1KCIS-optimized geometries of $Xe(OH)_4$, $XeO(OH)_3^-$, and $XeO_2(OH)_2^{2-}$, shown in Figure 1, demonstrate that the bond length between Xe and the oxygen atom of the OH^- group is longer than that between Xe and O^{2-}. Moreover, the *trans* effect of O^{2-} is stronger than that of OH^-. For example, the bond length between Xe and the O atom of the OH^- group increases from 2.103 Å in $Xe(OH)_4$ to 2.349 Å in $XeO(OH)_3^-$. Three minima were located on the $XeO_2(OH)_2^{2-}$ potential energy surface; one isomer has the two OH groups present in the *trans* position with respect to each

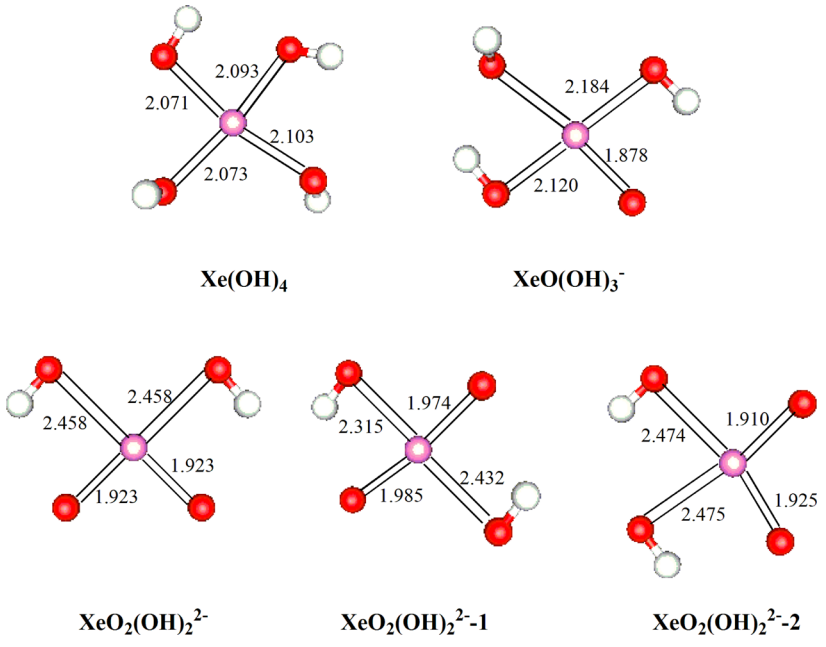

Figure 1. Converged geometries of $XeO_n(OH)_{4-n}^{n-}$ at the TPSS1KCIS/aug-cc-pVTZ(-PP) theoretical level (n = 0, 1, and 2; bond lengths are in angstroms).

dx.doi.org/10.1021/jp304434f | J. Phys. Chem. A 2012, 116, 10397−10402

Table 1. Calculated Electronic Energies (hartrees), Dipole Moments (D), Vibrational Frequencies (cm^{-1}), and Rotational Constants (GHz) of $XeO_n(OH)_{4-n}^{n-}$ (n = 0, 1, and 2)

	$Xe(OH)_4$	$XeO(OH)_3^-$	$XeO_2(OH)_2^{2-}$	$XeO_2(OH)_2^{2-}$-1	$XeO_2(OH)_2^{2-}$-2
calcd electronic energy[a]	−632.35521	−631.81843	−631.09109	−631.061045	−631.089671
dipole moment	1.53	1.12	3.13	0.38	3.13
vibrational frequency[b]			124	61	103
	87	96	124		109
	138	139	164	100	137
	153	168	215	121	193
			248	200	237
	198	214	254	208	248
	201	228	294	258	281
	233	274	391	299	287
	252	307	392	409	357
	268	325	603	500	597
			626	540	627
	330	400	753	573	695
	433	462	759	840	733
	464	582	3782	983	3778
	508	660	3782	3676	3788
		682		3743	
	510	916			
	918	1071			
	947	3616			
	977	3756			
	1003	3803			
	3727				
	3757				
	3765				
	3767				
rotational constant	3.34	3.85	3.59	4.2	3.18
	3.28	2.79	2.76	2.56	3.05
	1.67	1.62	1.56	1.59	1.56

[a]Values include the zero-point energies. [b]Values are uncorrelated by a scaling factor.

other (designated as $XeO_2(OH)_2^{2-}$-1 in Figure 1), whereas in the other two isomers, $XeO_2(OH)_2^{2-}$ and $XeO_2(OH)_2^{2-}$-2 (Figure 1), the OH groups are *cis* with respect to each other. The difference between these two isomers is the hydrogen-bonding mode. The isomer designated as $XeO_2(OH)_2^{2-}$ in Figure 1 has two O−H···O^{2-} hydrogen bonds. The average length of the O−H···O^{2-} hydrogen bonds in $XeO_2(OH)_2^{2-}$ is 2.413 Å. However, one O−H···O(−H) hydrogen bond and one O−H···O^{2-} hydrogen bond are present in the isomer designated as $XeO_2(OH)_2^{2-}$-2 in Figure 1. In $XeO_2(OH)_2^{2-}$-2, the lengths of the O−H···O(−H) and O−H···O^{2-} hydrogen bonds are 2.633 and 2.492 Å, respectively. Taking into account the calculated zero-point energy, $XeO_2(OH)_2^{2-}$ is more stable than $XeO_2(OH)_2^{2-}$-2 by approximately 4 kJ/mol. The calculated electronic energies, the dipole moments, the uncorrelated vibrational frequencies, and the rotational constants of $XeO_n(OH)_{4-n}^{n-}$ (n = 0, 1, and 2) are listed in Table 1. Given that the calculated dipole moments are nonzero in all cases, the species are all polar. Fewer negative charges for a species indicate increased stability. The three conformers of $XeO_2(OH)_2^{2-}$ exhibit a stability trend following the order $XeO_2(OH)_2^{2-}$ > $XeO_2(OH)_2^{2-}$-2 > $XeO_2(OH)_2^{2-}$-1. Furthermore, the stabilities of the dianions ($XeO_2(OH)_2^{2-}$, $XeO_2(OH)_2^{2-}$-1, and $XeO_2(OH)_2^{2-}$-2) were investigated using the autodetachment of an electron. For example, in $XeO_2(OH)_2^{2-}$, the autodetachment of an electron can be represented as follows:

$$XeO_2(OH)_2^{2-} \rightarrow XeO_2(OH)_2^{-} + e^- \quad (1)$$

On the basis of the TPSS1KCIS/aug-cc-pVTZ(-PP) theoretical level, the respective ΔH values for the autodetachment of an electron are −178, −238, and −178 kJ/mol for $XeO_2(OH)_2^{2-}$, $XeO_2(OH)_2^{2-}$-1, and $XeO_2(OH)_2^{2-}$-2. $XeO_2(OH)_2^{-}$, $XeO_2(OH)_2^{-}$-1, and $XeO_2(OH)_2^{-}$-2 are anionic radicals. The eigenvalue of S^2 was calculated to be approximately 0.75 for these anionic radicals, which is the expected value for a radical, indicating that the spin contamination is minor in this study. The calculated Xe−O bond lengths, and the hydrogen-bond length in the $XeO_2(OH)_2^{2-}$, $XeO_2(OH)_2^{2-}$-1, or $XeO_2(OH)_2^{2-}$-2 species and their corresponding electron-detachment products, are shown in Table 2; the Xe−O bond lengths increase on moving from x = −1 to −2 among the three conformers.

3.2. Comparison of $XeO_n(OH)_{4-n}^{n-}$ (n = 0, 1, and 2) with XeO_4. NBO analyses of $XeO_n(OH)_{4-n}^{n-}$ (n = 0, 1, and 2) and XeO_4 were performed at the TPSS1KCIS/aug-cc-pVTZ(-PP) theoretical level; the results are shown in Table 3. Natural population analysis of Xe predicted that this element has a positive charge which is smaller than its oxidation number (+4 or +8). The order of the bond between Xe(IV) and the O^{2-} anion is higher than that between Xe(IV) and the OH group, possibly because the *trans* effect of the O^{2-} anion is stronger than that of the OH group. The order of the bond between xenon and the hydroxyl group that is *trans* with respect to the

dx.doi.org/10.1021/jp304434f | J. Phys. Chem. A 2012, 116, 10397−10402

Table 2. Calculated Bond Lengths of Xe−O and Hydrogen-Bond Lengths (Å) for $XeO_2(OH)_2^{x-}$, $XeO_2(OH)_2^{x-}$-1, and $XeO_2(OH)_2^{x-}$-2 (x = 1 and 2)

	$XeO_2(OH)_2^{x-}$		$XeO_2(OH)_2^{x-}$-1		$XeO_2(OH)_2^{x-}$-2	
x	1	2	1	2	1	2
Xe−O(H) bond length	2.224	2.458	2.153[a]	2.374[a]	2.236[a]	2.475[a]
Xe−O bond length	1.883	1.923	1.935[a]	1.980[a]	1.878[a]	1.918[a]
O−H···O(−H) length					2.238	2.633
O−H···O^{2-} length	2.427[a]	2.413[a]	2.370[a]	2.290[a]	2.532	2.492

[a]Values are averages.

O^{2-} anion decreases from 0.3061 in $Xe(OH)_4$ to 0.1945 in $XeO(OH)_3^-$; furthermore, the order of the Xe−O bond is higher in XeO_4, as shown in Table 3. On the basis of our results, although $Xe(OH)_4$ is unstable with respect to Xe + $2H_2O_2$ by 251 kJ/mol, this does not influence the accuracy of the comparisons among the four-oxygen-bound Xe(IV) and Xe(VIII) species.

One method of synthesizing xenon tetroxide is a two-step reaction in which barium perxenate (Ba_2XeO_6) is first reacted with sulfuric acid:

$$Ba_2XeO_6 + 2H_2SO_4 \rightarrow 2BaSO_4 + H_4XeO_6 \quad (2)$$

In the second step, xenon tetroxide is obtained by dehydration of the unstable perxenic acid:[32]

$$H_4XeO_6 \rightarrow 2H_2O + XeO_4 \quad (3)$$

The reaction enthalpy of the second step of this reaction (eq 3) and the probability of perxenic acid undergoing the redox reaction shown in eq 4 were evaluated as described below.

$$H_4XeO_6 \rightarrow Xe(OH)_4 + O_2(^3\Sigma_g) \quad (4)$$

In the redox reaction in eq 4, two oxygen atoms are oxidized from the −2 valence state to 0 valence, whereas xenon is reduced from +8 to +4. The product $Xe(OH)_4$ is then dehydrated to give XeO_2 and water. The reactions of H_4XeO_6 considered herein are summarized in Scheme 3. Using the TPSS1KCIS functional, four minima were obtained on the H_4XeO_6 potential energy surface (ascribed to the conformers labeled H_4XeO_6, H_4XeO_6-1, H_4XeO_6-2, and H_4XeO_6-3). The geometric parameters of the conformers of H_4XeO_6 are shown in Figure 2, which illustrates that the Xe−O^{2-} bond is also, in this case, shorter than the Xe−OH bond. Like the conformers of $XeO_2(OH)_2$, the conformers of H_4XeO_6 can also be distinguished on the basis of the difference in their hydrogen-bonding patterns. On the basis of X-ray diffraction data, complete structures have been reported for $Na_4XeO_6·6H_2O$, $Na_4XeO_6·8H_2O$, and $K_4XeO_6·9H_2O$. In all of these hydrated perxenates, the XeO_6^{4-} ion adopts an octahedral conformation with Xe−O bond lengths of 1.84−1.86 Å and O−Xe−O angles of 87−93°.[33,34] The calculated energies, vibrational frequencies, dipole moments, and rotational constants of the conformers of H_4XeO_6 are summarized in Table 4. A higher calculated dipole moment indicates that the positively charged center is more distant from the negatively charged center in the molecule. Accordingly, the distances between the positively charged and negatively charged centers in the conformers follow the trend H_4XeO_6 > H_4XeO_6-1 > H_4XeO_6-3 > H_4XeO_6-2 (Table 4). In-depth inspection of the data in Table 4 shows that the relative stability of these conformers is in the order H_4XeO_6-3 > H_4XeO_6-2 > H_4XeO_6 > H_4XeO_6-1. The calculated reaction enthalpies of the reactions shown in Scheme 3 with respect to the conformers of H_4XeO_6 are summarized in Table 5. The data presented in Table 5 indicate that there is a correlation between the stability of the conformers of H_4XeO_6 and the heat evolved in the reactions represented in eqs 3 and 4. The higher stability of the conformer of H_4XeO_6 results in these reactions

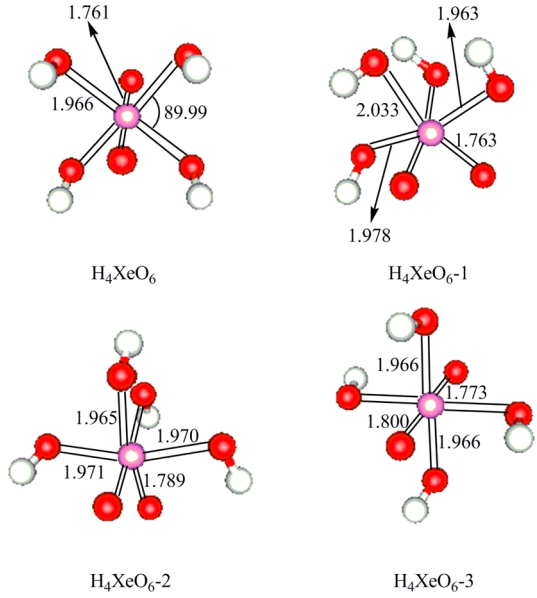

Figure 2. TPSS1KCIS-optimized geometries of the conformers H_4XeO_6, H_4XeO_6-1, H_4XeO_6-2, and H_4XeO_6-3 (bond lengths in angstroms, bond angles in degrees).

Table 3. Results of NBO Analyses of $XeO_n(OH)_{4-n}^{n-}$ (n = 0, 1, and 2)

	q(Xe)	q(O)	q(O(−H))[a]	bond order of Xe−O[b]	bond order of Xe−O(−H)[a]
$Xe(OH)_4$	1.975		−0.9542		0.3636
$XeO(OH)_3^-$	1.900	−1.029	−1.051	0.6616	0.3061
					0.1945[c]
$XeO_2(OH)_2^{2-}$	1.854	−1.115	−1.175	0.5957	0.1566
$XeO_2(OH)_2^{2-}$-1	1.731	−1.154	−1.069	0.5278	0.1945
$XeO_2(OH)_2^{2-}$-2	1.849	−1.107	−1.182	0.8983	0.2108
XeO_4	3.381	−0.8452		0.7981	

[a]O atom in the OH group. [b]Values based on the atom−atom overlap-weighted natural atomic orbitals. [c]The OH group is located in the *trans* position at O^{2-}.

dx.doi.org/10.1021/jp304434f | J. Phys. Chem. A 2012, 116, 10397−10402

Table 4. Calculated Energies (hartrees), Vibrational Frequencies (cm^{-1}), Dipole Moments (D), and Rotational Constants (GHz) of Conformers of H_4XeO_6

	H_4XeO_6	H_4XeO_6-1	H_4XeO_6-2	H_4XeO_6-3
calcd energy[a]	−782.614790	−782.613080	−782.615624	−782.617822
vibrational frequency[b]	181	175	204	192
	209	206	208	205
	214	213	224	217
	214	248	228	274
	291	293	271	281
	296	301	289	300
	296	317	305	304
	303	327	323	330
	353	336	336	352
	353	345	340	355
	381	367	362	382
	382	372	371	384
	430	448	397	414
	530	498	526	530
	538	527	529	535
	595	545	551	594
	595	585	587	595
	744	806	808	767
	861	863	840	843
	1065	1035	1070	1079
	1078	1077	1102	1088
	1078	1112	1128	1093
	1167	1137	1136	1165
	3702	3696	3689	3697
	3704	3699	3691	3698
	3704	3708	3703	3700
	3710	3720	3712	3707
dipole moment	4.40	4.05	2.06	2.21
rotational constant	2.11	2.10	2.12	2.12
	2.11	2.02	2.01	2.11
	1.89	1.97	1.99	1.89

[a]Values include zero-point energies. [b]Values are uncorrelated by a scaling factor.

Table 5. Heats (ΔH_r, kJ/mol) of Reactions Presented in Eqs 3 and 4 and Dehydration of $Xe(OH)_4$

	ΔH_r of eq 3	ΔH_r of eq 4	ΔH_r for dehydration of $Xe(OH)_4$
H_4XeO_6	−34	−320	47
H_4XeO_6-1	−39	−325	47
H_4XeO_6-2	−32	−318	47
H_4XeO_6-3	−26	−312	47

being less exothermic. H_4XeO_6-3 is the most stable conformer and, thus, exhibits the lowest exothermicity in terms of these reactions among the conformers. As shown in Table 5, from the thermodynamic perspective, H_4XeO_6 may undergo the redox reaction represented in eq 4. Notably, the addition of the diffuse functions does not influence the geometry of XeO_2. Changing the basis set from cc-pVTZ(-PP) to aug-cc-pVTZ(-PP) does not change the Xe−O bond length and the O−Xe−O bond angle from the respective values of 1.851 Å and 113.7°. However, as mentioned, $Xe(OH)_4$ is unstable with respect to Xe + $2H_2O_2$; its formation may be followed by possible pathways.

3.3. Comparisons of $XeO_n(OH)_{4-n}^{n-}$ (n = 0, 1, and 2) and XeF_4. On the basis of VSEPR, $XeO_n(OH)_{4-n}^{n-}$ adopts a square-planar geometry, and two lone pairs are localized on the central xenon atom (see Scheme 2). The hybridization of the

Scheme 2. VSEPR Description of the Local Geometry of XeO_4

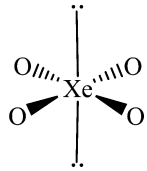

Scheme 3. Reactions of Perxenic Acid Considered in This Study

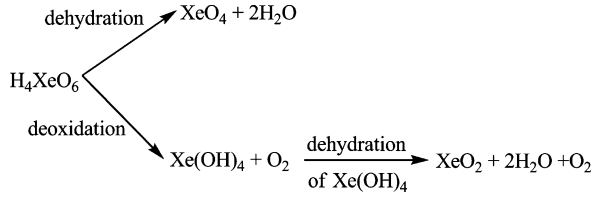

xenon atom required to generate the lone pairs can be also obtained using NBO analysis. These results are shown in Table 6; the lone pairs of electrons on xenon arise from hybridization

Table 6. Hybridization of Lone Pairs and Natural Electronic Configurations of Xe [Based on TPSS1KCIS/aug-cc-PVTZ(-PP)]

	hybridization of lone pairs on Xe	natural electronic configuration of Xe
$Xe(OH)_4$	$sp^{0.01}d^{0.00}f^{0.00}$	$[Kr]\,5s^{1.99}5p^{3.91}4f^{0.01}5d^{0.08}6p^{0.01}7s^{0.02}$
	$sp^{96.31}d^{0.01}f^{0.00}$	
$XeO(OH)_3^-$	$sp^{0.68}d^{0.00}f^{0.00}$	$[Kr]\,5s^{1.95}5p^{4.03}6s^{0.02}4f^{0.01}5d^{0.08}6p^{0.01}$
	$sp^{1.79}d^{0.00}f^{0.00}$	
$XeO_2(OH)_2^{2-}$	$sp^{1.00}d^{0.00}f^{0.00}$	$[Kr]\,5s^{1.91}5p^{4.10}6s^{0.02}4f^{0.01}5d^{0.08}6p^{0.02}$
	$sp^{0.09}d^{0.00}f^{0.00}$	
$XeO_2(OH)_2^{2-}$-1	$sp^{1.00}d^{0.00}f^{0.00}$	$[Kr]\,5s^{1.98}5p^{4.15}6s^{0.03}4f^{0.01}5d^{0.09}6p^{0.01}$
	$sp^{0.01}d^{0.00}f^{0.00}$	
$XeO_2(OH)_2^{2-}$-2	$sp^{1.00}d^{0.00}f^{0.00}$	$[Kr]\,5s^{1.92}5p^{4.10}6s^{0.02}4f^{0.01}5d^{0.08}6p^{0.02}$
	$sp^{0.09}d^{0.00}f^{0.00}$	
XeF_4	$sp^{0.00}d^{0.00}$	$[Kr]\,5s^{1.99}5p^{3.59}6s^{0.02}4f^{0.01}5d^{0.08}6p^{0.01}$
	$sp^{1.00}d^{0.00}f^{0.00}$	

of the s and p orbitals primarily. Conversely, the d and f orbitals of Xe make negligible contributions to the formation of the lone pairs on xenon. The natural electronic configuration of xenon in each species is also shown in Table 6; the 5s and 5p orbitals are the main contributors to the electronic configuration of Xe in these species. NBO analysis of the well-known square-planar molecule XeF_4 was also performed. These results are also listed in Table 6 for comparison with those of $XeO_n(OH)_{4-n}^{n-}$ (n = 0, 1, and 2). As shown in Table 6, the lone pairs of electrons on Xe in XeF_4 are also derived from the s and p orbitals of Xe. The xenon atom in XeF_4 has an electronic

dx.doi.org/10.1021/jp304434f | J. Phys. Chem. A 2012, 116, 10397−10402

configuration which is similar to that in $XeO_n(OH)_{4-n}^{n-}$ (n = 0, 1, and 2). On the basis of the TPSS1KCIS-converged geometry, XeF_4 assumes a square-planar geometry with a Xe−F bond length of 1.969 Å and F−Xe−F bond angle of 90°. These results are congruent with previous results (1.92 ± 0.03 Å and 90°).[35] The heat of formation was calculated to be −216 kJ/mol, which is within a relative error of 0.1413 with respect to the previous value (−251 kJ/mol).

4. CONCLUSIONS

From the DFT analysis of $XeO_n(OH)_{4-n}^{n-}$ (n = 0, 1, and 2), several conclusions were drawn as follows.

(1) Although the monomeric form of XeO_2 was calculated to be 516 kJ/mol less stable than the Xe atom and O_2, there is at least one minimum on the potential energy surface of $XeO_n(OH)_{4-n}^{n-}$ (n = 0, 1, and 2).
(2) Natural population analysis shows that the xenon atom has a positive charge that is smaller than its oxidation number of +4 or +8.
(3) Using the correlation between bond order and bond strength, bonding between Xe and the O^{2-} species was predicted to be stronger than that between Xe and OH^- in the series $XeO_n(OH)_{4-n}^{n-}$ (n = 0, 1, and 2). Furthermore, the order of the Xe−O^{2-} bond is higher in XeO_4 than in the aforementioned species.
(4) On the basis of DFT analysis at the TPSS1KCIS/aug-cc-pVTZ(-PP) level, the unstable perxenic acid (H_4XeO_6) may undergo deoxidation to produce $Xe(OH)_4$ and O_2.
(5) The 5s and 5p orbitals are the primary contributors to the electronic configuration of xenon, whereas the lone pair of electrons on the Xe atoms is mainly derived from the s and p orbitals. NBO analysis indicated a similar situation for XeF_4.

A more detailed understanding of the chemical properties of noble gases is essential to extend their applications. The data presented herein furnish further insights into the chemical reactivity of xenon.

■ ASSOCIATED CONTENT

Supporting Information

Optimization of the chosen DFT functionals, geometrical parameters of monomeric XeO_2 based on the chosen methods in this study, calculated ΔH_{form} and ΔH_{atom} of XeO_2, and TPSS1KCIS-calculated Xe−O bond length, ∠O−Xe−O, ΔH_{form}, and ΔH_{atom} of XeO_4. This material is available free of charge via the Internet at http://pubs.acs.org.

■ AUTHOR INFORMATION

Corresponding Author

*E-mail: chlai125@csmu.edu.tw.

Notes

The authors declare no competing financial interest.

■ ACKNOWLEDGMENTS

I am grateful to the National Center for High-Performance Computing in Taiwan for providing a generous amount of computing time. Financial support from the National Science Council of Taiwan is also gratefully acknowledged.

■ REFERENCES

(1) Dunkin, I. R. *Chem. Soc. Rev.* **1980**, *9*, 1.
(2) Häussinger, P.; Glatthaar, R.; Rhode, W.; Kick, H.; Benkmann, C.; Weber, J.; Wunschel, H-J; Stenke, V.; Leicht, E.; Stenger, H. In *Ullmann's Encyclopedia of Industrial Chemistry*; Bellussi, G., Bohnet, M., Bus, J., Eds.; Wiley-VCH: Weinheim, Germany, 2002.
(3) Basting, D.; Marowsky, G. *Excimer Laser Technology*; Springer: Berlin, Germany, 2005.
(4) Graham, L.; Graudejus, O.; Jha, N. K.; Bartlett, N. *Coord. Chem. Rev.* **2000**, *197*, 321.
(5) Sanloup, C.; Schmidt, B. C.; Chamorro Perez, E. M.; Jambon, A.; Gregoryanz, E.; Mohamed Mezouar, M. *Science* **2005**, *310*, 1174.
(6) Brock, D. S.; Schrobilgen, G. J. *J. Am. Chem. Soc.* **2011**, *133*, 6265.
(7) Kunz, J.; Staudacher, T.; Allegre, C. J. *Science* **1998**, *280*, 877.
(8) Ozima, M.; Podosek, F. A. *J. Geophys. Res.* **1999**, *104*, 25493.
(9) Wacker, J. F.; Anders, E. *Geochim. Cosmochim. Acta* **1984**, *48*, 2373.
(10) Sill, G. T.; Wilkening, L. L. *Icarus* **1978**, *33*, 13.
(11) Matsuda, J-I; Matsubara, K. *Geophys. Res. Lett.* **1989**, *16*, 81.
(12) Pepin, R. O. *Icarus* **1991**, *92*, 2.
(13) Frisch, M. J.; Trucks, G. W.; Schlegel, H. B.; Scuseria, G. E.; Robb, M. A.; Cheeseman, J. R.; Montgomery, Jr., J. A.; Vreven, T.; Kudin, K. N.; Burant, J. C.; et al. *Gaussian 03*, revision C.02; Gaussian, Inc.: Wallingford, CT, 2004.
(14) Head-Gordon, M.; Pople, J. A.; Frisch, M. J. *Chem. Phys. Lett.* **1988**, *153*, 503.
(15) Becke, A. D. *Phys. Rev. A: At., Mol., Opt. Phys.* **1988**, *38*, 3098.
(16) Lee, C.; Yang, W.; Parr, R. G. *Phys. Rev. B: Condens. Matter Mater. Phys.* **1988**, *37*, 785.
(17) Dahlke, E. E.; Truhlar, D. G. *J. Phys. Chem. B* **2005**, *109*, 15677.
(18) Schultz, N.; Zhao, Y.; Truhlar, D. G. *J. Phys. Chem. A* **2005**, *109*, 11127.
(19) Zheng, J.; Zhao, Y.; Truhlar, D. G. *J. Chem. Theory Comput.* **2009**, *5*, 808.
(20) Tao, J.; Perdew, J. P.; Staroverov, V. N.; Scuseria, G. E. *Phys. Rev. Lett.* **2003**, *91*, 146401.
(21) Becke, A. D. *J. Chem. Phys.* **1993**, *98*, 5648.
(22) Adamo, C.; Barone, V. *J. Chem. Phys.* **1998**, *108*, 664.
(23) Lynch, B. J.; Fast, P. L.; Harris, M.; Truhlar, D. G. *J. Phys. Chem. A* **2000**, *104*, 4811.
(24) Staroverov, V. N.; Scuseria, G. E.; Tao, J.; Perdew, J. P. *J. Chem. Phys.* **2003**, *119*, 12129.
(25) Zhao, Y.; Lynch, B. J.; Truhlar, D. G. *J. Phys. Chem. A* **2004**, *108*, 2715.
(26) Zhao, Y.; Truhlar, D. G. *J. Phys. Chem. A* **2004**, *108*, 6908.
(27) Zhao, Y.; Lynch, B. J.; Truhlar, D. G. *Phys. Chem. Chem. Phys.* **2005**, *7*, 43.
(28) Dunning, T. H., Jr. *J. Chem. Phys.* **1989**, *90*, 1007.
(29) Peterson, K. A.; Figgen, D.; Goll, E.; Stoll, H.; Dolg, M. *J. Chem. Phys.* **2003**, *119*, 11113.
(30) Zhu, L.; Bozzelli, J. W. *Chem. Phys. Lett.* **2002**, *362*, 445.
(31) Reed, A. E.; Curtiss, L. A.; Weinhold, F. *Chem. Rev.* **1988**, *88*, 899.
(32) Klaening, U. K.; Appelman, E. H. *Inorg. Chem.* **1988**, *27*, 3760.
(33) Zalkin, A.; Forrester, J. D.; Templeton, D. H. *Inorg. Chem.* **1964**, *3*, 1417.
(34) (a) Ibers, J. A.; Hamilton, W. C.; MacKenzie, D. R. *Inorg. Chem.* **1964**, *3*, 1412. (b) Zalkin, A.; Forrester, J. D.; Templeton, D. H.; Williamson, S. M.; Koch, C. W. *J. Am. Chem. Soc.* **1964**, *86*, 3569.
(35) Ibers, J. A.; Hamilton, W. C. *Science* **1963**, *139*, 106.

■ NOTE ADDED AFTER ASAP PUBLICATION

This paper was published ASAP on October 2, 2012. The graphical abstract was revised, and the revised version of the paper was reposted on October 9, 2012.

國科會補助計畫衍生研發成果推廣資料表

日期:2013/12/23

國科會補助計畫	計畫名稱: 密度泛函數理論(DFT)對於一些化學系統的精確性
	計畫主持人: 賴金宏
	計畫編號: 101-2113-M-040-004- 學門領域: 理論與計算化學

無研發成果推廣資料

101 年度專題研究計畫研究成果彙整表

計畫主持人：賴金宏	計畫編號：101-2113-M-040-004-
計畫名稱：密度泛函數理論(DFT)對於一些化學系統的精確性	

成果項目			量化			單位	備註（質化說明：如數個計畫共同成果、成果列為該期刊之封面故事...等）
			實際已達成數（被接受或已發表）	預期總達成數(含實際已達成數)	本計畫實際貢獻百分比		
國內	論文著作	期刊論文	1	0	100%	篇	
		研究報告/技術報告	0	0	100%		
		研討會論文	1	0	100%		
		專書	0	0	100%		
	專利	申請中件數	0	0	100%	件	
		已獲得件數	0	0	100%		
	技術移轉	件數	0	0	100%	件	
		權利金	0	0	100%	千元	
	參與計畫人力（本國籍）	碩士生	0	0	100%	人次	
		博士生	0	0	100%		
		博士後研究員	0	0	100%		
		專任助理	0	0	100%		
國外	論文著作	期刊論文	0	0	100%	篇	
		研究報告/技術報告	0	0	100%		
		研討會論文	0	0	100%		
		專書	0	0	100%	章/本	
	專利	申請中件數	0	0	100%	件	
		已獲得件數	0	0	100%		
	技術移轉	件數	0	0	100%	件	
		權利金	0	0	100%	千元	
	參與計畫人力（外國籍）	碩士生	0	0	100%	人次	
		博士生	0	0	100%		
		博士後研究員	0	0	100%		
		專任助理	0	0	100%		

其他成果 (無法以量化表達之成果如辦理學術活動、獲得獎項、重要國際合作、研究成果國際影響力及其他協助產業技術發展之具體效益事項等，請以文字敘述填列。)	此篇論文在去年(2012 年)發表，其中的結果已被今年由英國皇家化學會(the Royal Chemical Society)所出版的 Annual Reports Section ’’ A’’ (Inorganic Chemistry)中的一篇論到稀有氣體的化學之論文所引用。1 可見此篇論文中的結果具有一定的影響力。 Reference: 1. Brocka, D. S. and Schrobilgen, G. J. Annu. Rep. Prog. Chem., Sect. A: Inorg. Chem. 2013,109, 101-107.

	成果項目	量化	名稱或內容性質簡述
科教處計畫加填項目	測驗工具(含質性與量性)	0	
	課程/模組	0	
	電腦及網路系統或工具	0	
	教材	0	
	舉辦之活動/競賽	0	
	研討會/工作坊	0	
	電子報、網站	0	
	計畫成果推廣之參與（閱聽）人數	0	

國科會補助專題研究計畫成果報告自評表

請就研究內容與原計畫相符程度、達成預期目標情況、研究成果之學術或應用價值（簡要敘述成果所代表之意義、價值、影響或進一步發展之可能性）、是否適合在學術期刊發表或申請專利、主要發現或其他有關價值等，作一綜合評估。

1. 請就研究內容與原計畫相符程度、達成預期目標情況作一綜合評估

■達成目標

□未達成目標（請說明，以 100 字為限）

□實驗失敗

□因故實驗中斷

□其他原因

說明：

2. 研究成果在學術期刊發表或申請專利等情形：

論文：■已發表 □未發表之文稿 □撰寫中 □無

專利：□已獲得 □申請中 ■無

技轉：□已技轉 □洽談中 ■無

其他：(以 100 字為限)

3. 請依學術成就、技術創新、社會影響等方面，評估研究成果之學術或應用價值（簡要敘述成果所代表之意義、價值、影響或進一步發展之可能性）(以 500 字為限)

此篇論文在去年(2012 年)發表，其中的結果已被今年由英國皇家化學會(the Royal Chemical Society)所出版的 Annual Reports Section ’’ A’’ (Inorganic Chemistry)中的一篇論到稀有氣體的化學之論文所引用。1 可見此篇論文中的結果具有一定的影響力。

Reference:

1. Brocka, D. S. and Schrobilgen, G. J. Annu. Rep. Prog. Chem., Sect. A: Inorg. Chem. 2013,109, 101-107.